An Extended Point-Area Deconvolution Approach for Assessing Drug Input Rates

Kuang C. Yeh,[1,2] Daniel J. Holder,[1] Gregory A. Winchell,[1] Larissa A. Wenning,[1] and Thomayant Prueksaritanont[1]

Received July 5, 2001; accepted July 10, 2001

Purpose. To describe an extended point-area deconvolution approach for evaluating drug input rates based on the application of piecewise cubic polynomial functions.

Methods. Both the nonimpulse response data and the impulse reference data were independently represented by the piecewise cubic polynomials to obtain interpolations, numerical integration, and reduced step size for the staircase input rates. A moving average algorithm was employed to compute the input rate estimates. The method was illustrated using data from preclinical and human studies. Simulations were used to examine the effects of data noise.

Results. In all cases examined, the piecewise cubic interpolation functions combined with the moving average algorithm yielded estimates that were reasonable and acceptable. Compared to the standard point-area approach based on the trapezoidal rule, the present method resulted in estimates that were closer to the expected values.

Conclusions. The point-area deconvolution analysis is one of the preferred approaches in assessing pharmacokinetic and biopharmaceutic data when it is undesirable to assume the functional forms of the input processes. The present method provides improved performance and greater flexibility of this approach.

KEY WORDS: point-area deconvolution; drug release; pharmacokinetics; biopharmaceutics; piecewise cubic interpolants; numerical integration.

INTRODUCTION

In a recent publication, a modified point-area numerical deconvolution procedure was used to investigate the kinetics of metabolite formation (1). A large number of different computational algorithms have been developed and used in the analysis of drug input rates in pharmacokinetic and biopharmaceutic studies (2–16). A general approach has been to assume an appropriate function for the plasma concentration data after intravenous administration and another for the input rate. The unit impulse response data after an i.v. administration are often represented by polyexponential functions. And the input functions are represented by polyexponentials, polynomials of various degrees, or other appropriate smoothing functions with adjustable parameters. The convolution of the two functions yields the nonintravenous response function, and the parameters are solved by nonlinear iterative regression analysis of the nonintravenous plasma data.

One of the alternative approaches that does not require predefined input functional form and the subsequent regression analysis is the point-area method based on the staircase input function (12–15). In this approach, the input rate is assumed to be piecewise constant within each sampled interval. The intravenous concentration data either are integrated numerically using the linear or log-linear trapezoidal rule, or are fit to polyexponential functions and integrated analytically. In actual practice, the sampled intervals are likely to be relatively large, and the input rate may vary substantially within such intervals, leading to large errors that are not representative of the system.

To reduce the inherent sensitivity of the point-area method to such errors, a modified procedure was developed to compute the drug input rates. It is the purpose of this paper to describe the application and limitations of the present method in the deconvolution analysis of pharmacokinetic and biopharmaceutic data.

METHODS

Deconvolution techniques have been well documented. Briefly, in a linear and time-invariant disposition system, the response function $g(t)$ is related to the input rate function $r(t)$ and the unit impulse response $c(t)$ by the following:

$$g(t) = r(t) * c(t) \tag{1}$$

or

$$g(t) = \int_0^t r(\tau)c(t-\tau)d\tau \tag{2}$$

where * denotes the convolution operation. In the present context, $c(t)$ generally represents the plasma concentrations following an i.v. bolus administration of a unit dose, $g(t)$ represents the corresponding concentrations following an oral or nonintravenous dose, and $r(t)$ is the drug input rate into the systemic circulation. The rate is expressed in fractions of the unit i.v. impulse dose per unit time. In Eq. 2, $t - \tau$ is the time lapsed between the time τ at which the drug input takes place and the time t ($t \geq \tau$) at which the response $g(t)$ is observed. The response $g(t)$ is, essentially, a summation of the products of the input rate and the time-shifted impulse response. As an inverse operation to convolution, the deconvolution allows one to obtain estimates of the input rate function $r(t)$ based on the observed $c(t)$ and $g(t)$ data.

In the present work, the step-size of the staircase input function is reduced to equal a fraction of the sampled time interval following nonintravenous administration. A piecewise cubic interpolation algorithm (17) is applied to obtain the interpolated values for the nonimpulse and unit-impulse response data. The point-area method is applied to obtain the cumulative input rates, followed by a moving average numerical differentiation algorithm to obtain the absorption rates at the observed time points.

Staircase Input Rate

Dividing the time interval $[0,t]$ into $(j - 1)$ sufficiently narrow subintervals such that within each subinterval h_k ($h_k = t_k - t_{k-1}$, $k = 2, 3, \ldots, j$), the input rate r_k is approximated to be constant. Under such approximation conditions, Eq. 2 can be written as:

[1] Merck Research Laboratories, West Point, PA 19486.

[2] To whom correspondence should be addressed. (e-mail: kuang.yeh@worldnet.att.net)

0724-8741/01/1000-1426$19.50/0

$$g_j \cong \sum_{k=2}^{j} \bar{r}_k \int_{t_{k-1}}^{t_k} c(t_j - \tau)d\tau,\ j > 1,\ t_1 = 0,\ g_1 = 0 \tag{3}$$

where

$$\bar{r}_k = \frac{1}{h_k} \int_{t_{k-1}}^{t_k} r(t)\, dt \tag{4}$$

and

$$g_j = g(t_j) \tag{5}$$

An integration of the plasma concentration data over each subinterval $[t_{k-1}, t_k]$ yields the area under the curve within that subinterval:

$$b_{jk} = \begin{cases} \int_{t_j - t_k}^{t_j - t_{k-1}} c(\tau)\, d\tau, k \le j \\ 0, \textit{otherwise} \end{cases} \tag{6}$$

With Eq. 6, Eq. 3 can be given as follows:

$$g_j = \sum_{k=2}^{j} \bar{r}_k b_{jk} \tag{7}$$

Equation 7 represents one of the equations in a system of (j – 1) simultaneous equations which, when solved recursively, results in a working expression for the average input rate r_j:

$$\bar{r}_j = \frac{g_j - \sum_{k=2}^{j-1} \bar{r}_k b_{jk}}{b_{jj}} \tag{8}$$

Expressions equivalent or similar to Eq. 8 have been reported previously (3,8,12). The method has been given the name of the point-area deconvolution where the point denotes $g(t)$ and the area denotes the integrated b_{jj} based on $c(t)$. As stated earlier, the step-size is equated to the sampled interval in the conventional approach.

An integration of $r(t)$ yields the cumulative absorption $a(t)$:

$$a_j = a(t_j) = \sum_{k=2}^{j} \bar{r}_k\, (t_k - t_{k-1}) \tag{9}$$

Piecewise Cubic Interpolation

In Eq. 8, the evaluation of $g(t)$ at t_j is achieved by data interpolation using the piecewise cubic polynomial algorithm (17). The algorithm, adapted from the one originally developed by Fritsch-Butland (18), provides a consistent and reliable interpolation for numerical integration, yielding area under the curve (AUC) estimates that are less biased than by the trapezoidal rule. These functions are able to produce interpolations without spurious oscillations. Interpolated functions based on this algorithm are smooth and are constrained to be differentiable only once at the joints where experimental data points are located (cubic splines are twice differentiable). The resultant constrained curvature has a rigidity that falls between that of the conventional trapezoidal, which is extremely rigid, and cubic splines, which is extremely flexible. Cubic splines and Lagrange functions (19) are not suitable for the present application due to their occasional propensity of producing unexpected oscillations in the presence of experimental errors, generating unreliable AUC values. Linear or log-linear trapezoidal interpolations are also not suitable for consistenly yielding biased AUC estimates, depending on the concavity of the curvature manifested in the data. Examples of such interpolated profiles are shown in Fig. 1.

Based on the above interpolation algorithm (17), the function g_j between two experimentally observed adjacent data points (x_{n-1}, y_{n-1}) and (x_n, y_n) is defined by the following cubic equation:

$$g_j = y_{n-1} + \dot{y}_{n-1}\,(t_j - x_{n-1}) + p_n(t_j - x_{n-1})^2 + q_n(t_j - x_{n-1})^3 \tag{10}$$

where

$$p_n = \frac{1}{d_n}(3s_n - 2\dot{y}_{n-1} - \dot{y}_n)$$

$$q_n = \frac{1}{d_n^2}(\dot{y}_{n-1} + \dot{y}_n - 2s_n)$$

$$d_n = x_n - x_{n-1}$$

$$s_n = \frac{y_n - y_{n-1}}{d_n}$$

$$x_{n-1} < t_j \le x_n$$

$\dot{y}_{n-1}$, $\dot{y}_n$ = slopes of the curve evaluated at x_{n-1} and x_n, respectively. The procedures for selecting these slopes have been studied and presented in an earlier report (17).

Unit-Impulse Response

In the present application, the unit impulse response is generally represented by the experimentally observed plasma concentrations $c(t)$ following i.v. administration. The evaluation of $c(t)$ at the time corresponding to t_j of $g(t)$ is achieved independently by interpolation of the $c(t)$ data using the above piecewise cubic polynomial algorithm (17), and the b_{jk} terms shown in Eq. 6 are subsequently obtained by Eq. 11 which is a modified trapezoidal method for numerical integration (17):

$$b_{jk} = \frac{h_k}{2}[c(t_j - t_k) + c(t_j - t_{k-1})] + \frac{h_k^2}{12}[\dot{c}(t_j - t_k) - \dot{c}(t_j - t_{k-1})] \tag{11}$$

Step-Size of the Stair-Case Input

While it is desirable that pharmacokinetic and biopharmaceutic studies include a sufficient number of plasma samplings to achieve adequate characterization of the plasma concentration profile, practical considerations often limit the number of sampled time points. To maximize the retrievable kinetic information, the sampled times are often optimally spaced such that the length of the sampled interval d_n is inversely, albeit qualitatively, related to the magnitude of the expected drug input rate and/or the magnitude of the expected fluctuations of plasma levels. The importance of optimal sampling strategy had been extensively reviewed (20). Typically, such considerations often lead to sampling times which are unequally spaced, and some intervals may be much greater than the step-size h_k required to satisfy the approximation assumption for Eq. 4.

To define the length of the step-size h_k, an approach that is adopted in the present method is to take advantage of the underlying assumption of the unequal sampling intervals, and

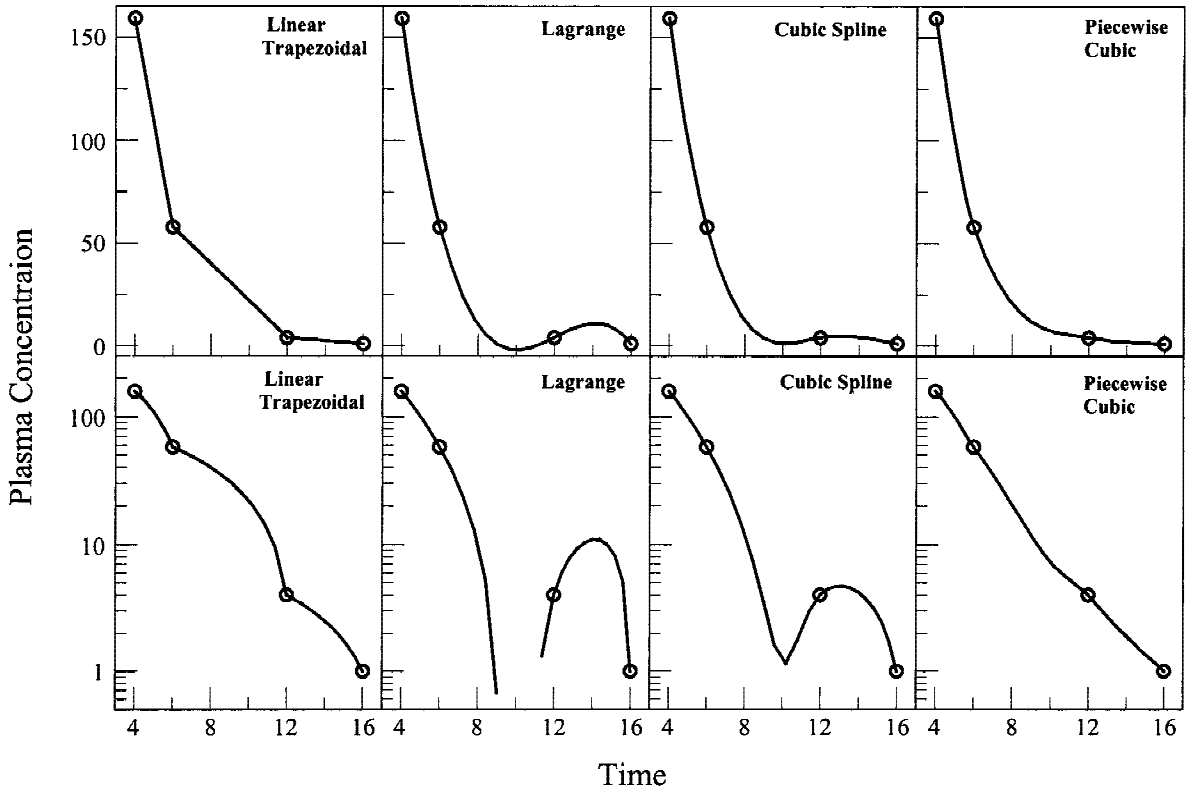

Fig. 1. A comparison of the four interpolated curves passing through 4 time points at (4,159), (6,58), (12,4), and (16, 1). Spurious oscillations produced by the Lagrange and spline method over the middle time interval are also shown. The semilog plots of the graphs are displayed in the lower panel.

set h_k to equal a fraction of each of the sampled interval d_n of the nonimpulse response data:

$$h_k = \frac{d_n}{f} \tag{12}$$

In Eq. 12, f is a working parameter that defines the number of subdivisions. With Eq. 12, each sampled interval d_n is divided into f-equally spaced subintervals such that the absorption rate r_k is assumed constant within the subinterval. The subscript parameter j in Eq. 8 is related to the subscript parameter n of the plasma sampling time as follows:

$$j = f(n-1) + 1, n = 2, 3, \ldots, N \tag{13}$$

where N is the total number of experimentally observed plasma data points.

Since the width of the interpolated subinterval h_k is proportional to each of the sampled interval d_n, the length of the subinterval for the b_{jj} term shown in the denominator of Eq. 8 varies with each d_n. Based on the assumption that d_n will increase with increasing time post-dosing, h_k will also increase proportionally and the width for b_{jk} at later time points may potentially exceed closely spaced earlier sampled intervals. In general, the working parameter f can be chosen to be equal to or less than the ratio of the largest sampled interval to the smallest sampled interval in the study:

$$f \leq \frac{d_N}{d_2} \tag{14}$$

This choice often yields an f value in the range of 1–20.

Absorption Rates

Based on the cumulative absorption $a(t)$ of Eq. 9, the cumulative absorption A_n at each sampled time x_n when $t_j = x_n$, is:

$$A_n = a_j, n = 2, 3, \ldots, N \tag{15}$$

For the interior points ($n = 2, 3, \ldots, N-1$), piecewise quadratic equations are fitted to the nearest three points (x_{n-1}, A_{n-1}), (x_n, A_n), and (x_{n+1}, A_{n+1}), forming a system of 3 linear equations with 3 unknowns:

$$A_{n-1} = u_n + v_n x_{n-1} + w_n x_{n-1}^2 \tag{16a}$$

$$A_n = u_n + v_n x_n + w_n x_n^2 \tag{16b}$$

$$A_{n+1} = u_n + v_n x_{n+1} + w_n x_{n+1}^2 \tag{16c}$$

The slope at A_n, denoted $\dot{A}_n$, is found by solving the above equations for u_n, v_n, and w_n,

$$\dot{A}_n = v_n + 2w_n x_n \tag{17}$$

If the computed slope is negative, then it is estimated to be zero.

The slope at the first sampled time point ($n = 1$), $\dot{A}_1$, is approximated by the input rate of the first subinterval, $\bar{r}_2$, and the slope at the final sampled time point ($n = N$), $\dot{A}_N$, is approximated by the input rate of the final sub-interval, $\bar{r}_j$, as defined in Eq. 8.

The drug input rate R_n at the sampled time x_n is estimated by the moving average of the three contiguous slope values,

$$R_n = \tfrac{1}{2}[\tfrac{1}{2}(\dot{A}_{n-1} + \dot{A}_n) + \tfrac{1}{2}(\dot{A}_n + \dot{A}_{n+1})],\ n = 2, 3, \ldots, N-1 \quad (18)$$

If the computed rate R_{N-1} at the sampled time point x_{N-1} is negative, then it is estimated to be zero. No constraints are imposed on R_n at other time points. As indicated in Eq. 18, the input rates are not computed at the first sampled time point x_1 and the last sampled time point x_N. Furthermore, input rates at the interpolated time points are not computed due to the imperfection of the numerical algorithm and the resultant lower reliability of the interpolated g_j's relative to the directly observed y_n's.

Computation

Computer software has been developed to implement the above procedures. Results of the experiments are shown below. The program contains specific subroutines to perform the following functions: receive the nonimpulse response concentration data $g(t)$; receive the unit impulse response concentration data $c(t)$; receive the subdivision parameter f; perform data interpolation n both nonimpulse and impulse response data and numerical integration; compute the cumulative input A_n and input rate R_n. The software has been compiled into a stand-alone program that runs on an IBM compatible PC in the DOS environment of Windows NT or 98. A modification of the present procedure where the unit impulse response data are represented by polyexponential equations has also been developed and implemented. This modified procedure is described in the Appendix.

Seven data cases were employed to illustrate the present method. In cases 1–4 (Table I), simulated data based on three defined absorption functions (Function 1: a first-order decay type; Function 2: a bipeak mixed drug-release type; and Function 3: a zero-order controlled-release type) and two unit impulse response functions (i.v. bolus in Data Cases 1–3, and oral solution in Data Case 4) were used. The nonimpulse response was represented by computed plasma concentrations following the analytical convolution of the impulse response function and the respective absorption function. Function 3 was tested in the fourth case where the unit impulse response was represented by plasma concentration data following the administration of an oral solution. Unit impulse response concentrations in all cases were sampled at 0, 0.1, 0.25, 0.5, 1, 1.5, 2, 3, 4, 6, 8, 10, and 12 h post-dose; an additional sample at 0.75 hours was collected in Case 4. Plasma concentrations following oral administration in Cases 1–3 were sampled at 0, 0.25, 0.5, 0.75, 1, 1.5, 2, 3, 4, 5, 6, 8, 10, and 12 h post-dose; additional samples were collected at 2.5, 3.5, and 4.5 h in Case 2, and at 7 and 9 h in Case 3. In Data Case 4, the plasma samples were collected hourly for 10 h and at 12 h. Normally distributed random noise corresponding to 5%, 10%, and 15% CV (coefficient of variation) were independently added into the simulated impulse response data and the nonimpulse response data. Ten (10) data sets were generated at each of the 3 noise levels and for each of the 4 cases. Each of the 120 paired test data sets was comprised of one set of the impulse response data and one set of the nonimpulse response data.

In Data Cases 5 and 6, the present method was applied to experimentally observed preclinical plasma concentration data of a fibrinogen receptor antagonist in the dog (1) and human quindine sustained-release formulation data (21), respectively. In Data Case 7, the present method was compared to a previously published point-area method (14). The nonimpulse response data included simulated noise-free plasma concentrations following oral administration (Calculation A), noise-free concentrations with an abbreviated sampling scheme (Calculation B), and plasma concentrations containing +10% and −10% noise at alternating time points (Calculation C). The computational procedures described in the Appendix were employed in Data Case 7 since the unit impulse response in the calculations was represented by a polyexponential equation as reported in the referenced publicatons (14).

The above deconvolution analyses were performed with the parameter f set to equal the ratio (d_N/d_2) as shown in Eq. 14. To examine the effect of the step-size, the analyses were

Table I. Simulated Absorption Functions Tested

Data Case	Absorption rate function[a,b]	Unit impulse response
1	Function 1 (first-order decay): $r(t) = [\ln(2)/2] \exp\{-[\ln(2)t/2]\}$	Plasma concentration data following an i.v. bolus[d]
2	Function 2 (bi-peak biexponential input)[c]: $r(t) = 0.7\,[\exp(-0.45t) - \exp(-0.45t/0.55)],\ 0 \leq t < 4$ $r(t) = 0.7\,[\exp(-0.45t) - \exp(-0.45t/0.55)] + 0.3\,\{\exp[-0.45(t-4)] - \exp[-0.45\,(t-4)/0.55]\},\ t \geq 4$	Plasma concentration data following an i.v. bolus[d]
3	Function 3 (zero-order controlled-release): $r(t) = 0.12,\ 0 \leq t < 6$ $r(t) = 0.12[3.5^2 - (t-6)^2]/(3.5^2),\ 6 \leq t < 9.5$ $r(t) = 0,\ t \geq 9.5$	Plasma concentration data following an i.v. bolus[d]
4	Function 3 (zero-order controlled release): (Same as in Data Case 3)	Plasma concentration data following administration of an oral solution[e]

[a] Parameters for each absorption function are normalized to yield a total cumulative absorption of 1 unit dose.
[b] Time unit = hour.
[c] 70% dose-release at 0 h; 30% dose-release at 4 h.
[d] Disposition function for the plasma concentration data: $c(t) = 9\exp(-0.8t) + 3\exp(-0.2t)$.
[e] Disposition function for the plasma concentration data: $c(t) = 10\exp(-0.5t) - 10\exp(-2t)$.

then repeated in all seven cases without reducing the step-size ($f = 1$).

RESULTS

Simulation Data

Table II lists the computed input rates R_n in Cases 1–4 for the noise-free test data. These results indicate that the theoretical profiles were well reproduced by the present method in all 4 cases. There were only minor differences between the expected and the recovered absorption rates, which can be attributed mainly to the imperfection of the numerical algorithm. Figure 2 summarizes results of the test data containing the simulated noises. On average, the expected profiles were also well recovered. These results indicate that as the noise in the input data increased from 5% CV to 15% CV, there was a corresponding increase in the variability of the output data. Stable and qualitatively similar estimates for absorption rates were obtained at $f = 1$ in all 4 cases (and also in all subsequent cases except for Data Case 6 described below). Smaller step-sizes generally improved the accuracy and precision of the estimates of cumulative absorption A_n. However, the improvements were modest. Finally, as the bulk of absorption approached completion, the precision for the computed A_n increased while the precision for R_n decreased in all 4 cases.

It should be noted that Eq. 18 assumes the input rates are continuous and differentiable at all times. For Function 2, where 30% of the simulated dose was released as a bolus at 4 h, this assumption was poor and resulted in an overestimation of R_n at 4 h. Similarly for Function 3, where the simulated dose release completed abruptly at 9.5 h, the assumption was also poor and the estmated R_n at 9.5 h (by inference from Table II and Fig. 2) were higher than expected in both Cases 3 and 4.

As shown in Eq. 8, the step size h_k has an overriding effect on the reliability of the b_{jj} term and the corresponding rate estimates. With larger step sizes, errors associated with the imperfection of assuming constant input rate within each subinterval will generally be the predominant factor. With smaller step sizes, experimental error combined with the imperfection of the numerical interpolation algorithm will increasingly become the major factor. While the stability of the computed R_n is significantly improved with the application of the moving average algorithm, small step-sizes in the presence of relatively large noises may still potentially result in unstable and physically meaningless rate estimates. With Function 3 where the absorption rate was constant over a 6-h interval, reducing the step-size in the presence of data noise was, as expected, not useful. Although the estimated input rates were remarkably stable for all Case 3 data sets, erratic and meaningless rate estimates were observed in some of the Case 4 data sets containing higher noises (10% and 15% CV) when the step-size was further reduced. The difference between these two data cases suggests that assay noise would have greater impact on the stability of the computed rate estimates if there was a greater resemblance between the time profile of the impulse response data and that of the nonimpulse response data.

Metabolite Formation

Results of Data Case 5 are shown in Table III. These data were part of that reported previously on the metabolite formation of a fibrinogen antagonist ester prodrug in the dog (1). In this example, the nonimpulse response was represented by the plasma concentrations of the active metabolite $D_c(t)$ after oral administration of the prodrug, and the impulse response was represented by the plasma concentrations of the active metabolite $D_a(t)$ following intravenous administration of the active metabolite. The input rate $r(t)$, denoted $R_{drug}(t)$, measured the overall rate of appearance of the active metabolite in the systemic circulation following oral administration of the prodrug:

$$D_c(t) = R_{drug}(t) * D_a(t) \tag{19}$$

Data shown in Table III are based on normalized dose

Table II. Comparison of the Theoretical Absorption Rate $r(t)$ and Recovered Absorption Rate R_n for the 4 Test Cases Based on Simulated Noise-Free Plasma Concentrations as the Input Data

Case 1			Case 2			Case 3			Case 4		
x_n, h	$r(t)$, h^{-1}	R_n, h^{-1}	x_n, h	$r(t)$, h^{-1}	R_n, h^{-1}	x_n, h	$r(t)$, h^{-1}	R_n, h^{-1}	x_n, h	$r(t)$, h^{-1}	R_n, h^{-1}
0.25	0.318	0.314	0.25	0.055	0.055	0.25	0.120	0.119	1	0.120	0.124
0.5	0.291	0.292	0.5	0.094	0.089	0.5	0.120	0.120	2	0.120	0.121
0.75	0.267	0.268	0.75	0.121	0.116	0.75	0.120	0.120	3	0.120	0.120
1	0.245	0.241	1	0.137	0.134	1	0.120	0.120	4	0.120	0.120
1.5	0.206	0.209	1.5	0.151	0.145	1.5	0.120	0.120	5	0.120	0.120
2	0.173	0.170	2	0.148	0.145	2	0.120	0.120	6	0.120	0.117
3	0.123	0.128	2.5	0.137	0.135	3	0.120	0.120	7	0.110	0.104
4	0.087	0.091	3	0.121	0.121	4	0.120	0.120	8	0.081	0.074
5	0.061	0.065	3.5	0.105	0.108	5	0.120	0.120	9	0.032	0.035
6	0.043	0.044	4	0.089	0.105	6	0.120	0.116	10	0	0.009
8	0.022	0.026	4.5	0.115	0.111	7	0.110	0.102	12	0	
10	0.011	0.013	5	0.121	0.113	8	0.081	0.074			
12	0.005		6	0.105	0.096	9	0.032	0.037			
			8	0.056	0.063	10	0	0.010			
			10	0.026	0.032	12	0				
			12	0.011							

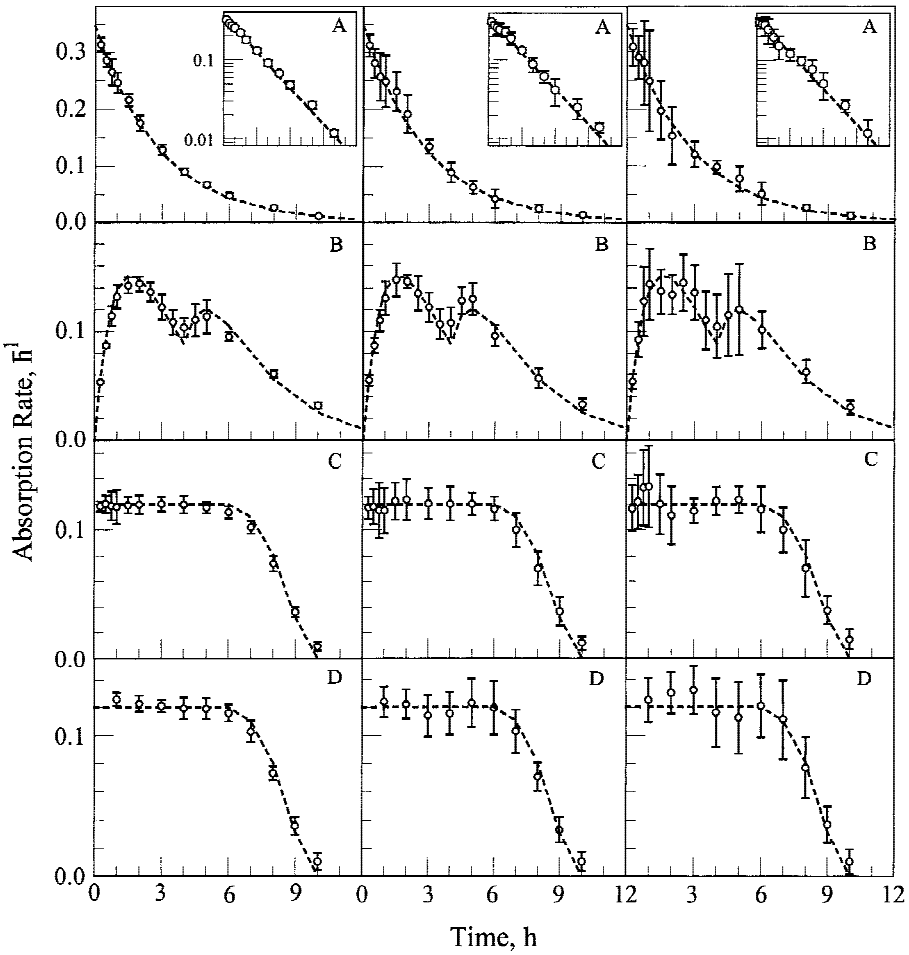

Fig. 2. Comparison of the theoretical and the recovered absorption rates at each of the three simulated noise levels in Case 1 (A), Case 2 (B), Case 3 (C), and Case 4 (D). The theoretical absorption rates are shown as the dashed lines. Vertical lines represent mean and one standard deviation of the results based on 10 paired data sets containing normally distributed random noise for both the nonimpulse response data and the unit impulse response data. The semilog plots of the absorption rates for Case 1 are shown in the insets. Left panel = 5% CV; middle panel = 10% CV; right panel = 15% CV.

and adjusted molecular weight of the prodrug and the active metabolite. Following oral administration of the prodrug, there were two pathways that led to the appearance of the metabolite in the systemic circulation: one was derived from the systemic conversion of the orally absorbed prodrug; the other derived from the direct contribution of the absorbed active metabolite as a result of the presystemic conversion during the absorption process. The computed $R_{drug}(t)$ profile (Fig. 3), which represents a composite of these two parallel pathways, would suggest that the formation of $D_c(t)$ was initially delayed, reached a peak at about 3–4 hours and decreased thereafter.

Table III. Estimated Composite Input Rate, R_{drug}, of the Active Metabolite in Data Case 5

Time, h	D_a, nM	D_c, nM	R_{drug}, h^{-1}	Cumulative R_{drug}
0	1546.25[a]	0		
0.25	903.25	NS[b]		
0.5	588.25	1.34	0.0056	0.0013
1	309.13	4.43	0.0118	0.0050
1.5	169.88	9.06	0.0204	0.0120
2	118.25	17.59	0.0291	0.0255
3	49.44	29.71	0.0347	0.0606
4	30.20	34.78	0.0348	0.0983
6	18.49	33.74	0.0301	0.1657
8	11.91	28.03	0.0227	0.2194
12	7.19	17.70		0.2879

Note: The unit impulse response was represented by the plasma concentrations of the metabolite D_a following intravenous administration of the metabolite. The nonimpulse response was represented by the plasma concentrations of the metabolite D_c following oral administration of the prodrug. Values have been dose-normalized to 0.1 mg/kg of the active metabolite.

[a] Value obtained by extrapolation prior to the application of deconvolution analysis.

[b] No sample.

Dosage Form Drug Release

Results of Data Case 6 are summarized in Table IV. In this example, the unit impulse response $c(t)$ was represented by the plasma concentrations of quinidine following the administration of an oral solution, and the nonimpulse response $g(t)$ was represented by the plasma concentration data following the administration of a sustained-release tablet (21). Thus, the input rate R_n is interpreted as the apparent *in vivo* release rate of the tablet formulation at the absorption sites

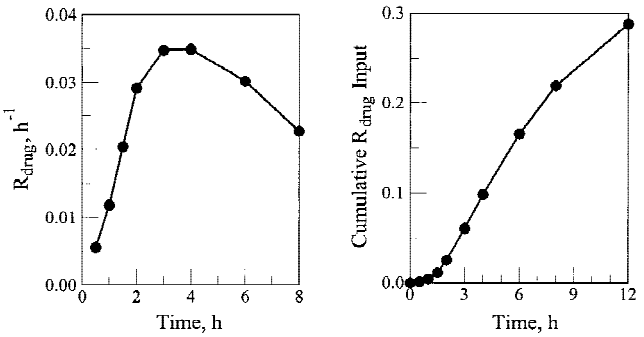

Fig. 3. Composite appearance rate (left panel) and cumulative rate (right panel) of the active metabolite following orally administered prodrug in the dog (Data Case 5).

projected to be equivalent to that of the oral solution. This application requires the assumption that linear and time-invariant kinetics apply not only to the disposition of quinidine in the systemic circulation, but also to its absorption processes at the sites where the drug is released from the dosage form. This example, similar to the simulation Case 4 above, further serves to illustrate the application of the present method where the impulse response is composed of plasma concentration data following a non-intravenous administration. Since $c(t_0) = 0$ at time zero, $\dot{g}(t_0)$ was also set to equal zero during data interpolation. These results suggest that the apparent drug release from the dosage form was rapid initially and the overall profile would be best described to be polyphasic. The cumulative absorption of 0.979 shown in Table V was comparable to the ratio 0.959 of the computed AUC values for the SR formulation (8,570 ng · h/mL) and for the oral solution (8,934 ng · h/mL).

In this example, extremely large step-size ($f = 1$) resulted in erratic and large fluctuations of the computed drug release rates at earlier time points, as shown in Table IV. However, with smaller step-size (Fig. 4), the magnitude of the fluctuations was substantially decreased and the computed release rates were generally comparable. The instability of the computed drug release rates at $f = 1$ suggests that the assumption of a constant rate over the earlier sampled time intervals (particularly the first interval) was poor, which was manifested by large decline of the initial drug release rates computed with the reduced step-sizes. The ruggedness of the present method is also suggested by the reasonable stability of computed drug release rates in this example with a modest reduction in the step-size ($f = 2$) and in all other data cases without reducing the step-size.

Comparative Data

Table V summarizes comparisons of the results in Data Case 7 and those previously published (14), using the procedures described in the Appendix. With the present method, improved and stable rate estimates were obtained in all three calculations and, unlike those results based on the conventional point-area method, no negative rates were generated in the presence of alternating 10% data noise.

DISCUSSION AND CONCLUSIONS

The above examples indicate that the reliability of the point-area method can be improved with the combined application of the moving average algorithm and the piecewise cubic polynominal functions. Allowing the step size to be adjustable in the method has the potential of yielding more meaningful drug input rate estimates. The stability of the resultant rate estimates, given the large variety of profiles examined in the above test data cases, also illustrated the flexibility of the method as a useful deconvolution tool. The computed absorption profiles may provide potential information for further investigation of the input processes. To date, no method has been reported on the use of such piecewise polynominal functions in representing both the impulse and non-impulse response data.

An important issue often encountered in numerical deconvolution is the presence of noise in the experimental data.

Table IV. Estimated *In Vivo* Drug Release Rates $R_n(t)$ of the Sustained Release (SR) Tablet Formation, Using Plasma Concentrtaions following the Administration of the Tablet and an Oral Solution (21)

Time, h	Plasma Concentration, ng/mL		*In Vivo* Release, h^{-1}		
	Oral Solution[a]	SR Tablet[a]	R_n ($f = 20$)	R_n ($f = 1$)	Cumulative R_n ($f = 20$)
0	0	0			–
0.5	685.6	243.3	0.973	0.317	0.181
1.0	923.9	242.7	0.143	0.060	0.233
2.0	897.0	313.9	0.109	0.120	0.362
3.0	677.2	347.1	0.098	0.097	0.462
4.0	620.3	376.0	0.082	0.085	0.550
6.0	399.8	451.1	0.056	0.066	0.734
8.0	381.4	367.0	0.035	0.033	0.764
10.0	298.1	364.1	0.025	0.027	0.848
12.0	242.2	326.7	0.015	0.016	0.878
24.0	97.1	142.4	0.006	0.005	0.960
36.0	40.1	62.4	0.001	0.001	0.974
46.0	25.9	36.2			0.979

Note: This application required the assumption of linear and time-invariant kinetics for the disposition of quinidine and absorption processes at the sites of drug release. Large step-size ($f = 1$) resulted in the drug release rates that were erratic and unrealistic over the initial sampled time intervals.

[a] Dose = 300 mg.

Table V. Comparison of Results Based on the Present Method and a Previously Reported Point-Area Method (14)

	Absorption Rate R_n, fraction of dose per hour[a]						
		Calculation A		Calculation B		Calculation C	
Time, h	Theoretical	Ref. 14[b]	Present work	Ref. 14[b]	Present work	Ref. 14[b]	Present work
0.25	0.583	0.635	0.580			0.571	0.594
0.5	0.490	0.534	0.483			0.705	0.515
1	0.347	0.412	0.350	0.491	0.374	0.270	0.334
2	0.173	0.245	0.206	0.246	0.211	0.343	0.187
3	0.087	0.123	0.105	0.123	0.104	0.018	0.103
4	0.043	0.061	0.053			0.155	0.053
5	0.022	0.030	0.027	0.043	0.042	−0.048	0.033
6	0.011	0.015	0.013			0.091	0.027
7	0.005	0.007	0.007	0.011	0.012	0.000	0.011
8	0.003	0.003	0.003			−0.037	0.001
9	0.001	0.002	0.002			0.034	0.000
10	0.001	0.000		0.002		−0.024	

[a] Calculation A was based on noise-free nonimpulse response data at the indicated time points; Calculation B was based on the noise-free data with the abbreviated sampling scheme; Calculation C was identical to Calculation A except that the nonimpulse response data contained +10% and −10% noise at alternating time points. In all calculations, the unit impulse response was represented by a biexponential equation: $5\exp(-0.5t)+5\exp(-0.2t)$.

[b] Mean absorption rate over the preceding sampled interval.

The input rates are particularly more sensitive than cumulative rates to such error. Unlike smoothing functions such as polyexponentials, interpolation functions do not filter out the noise and must reproduce the colocated experimental values. As a result, data-interpolation based deconvolution methods are inherently more sensitive to experimental noise than those based on data-smoothing algorithms, and fluctuations in input data will be more prominently reflected in the final output data. However, data smoothing before the deconvolution analyses generally requires great care to prevent the introduction of bias into the data. With the present method, the prior data smoothing operations are not required. The smoothing is performed on the slope of the computed cumulative absorption, and the difficulties generally associated with numerical differentiation are resolved by the application of the moving average algorithm. Obviously, the present method would not be applicable in situations where the fluctuations of the true input rates are such that they are not compatible with the assumptions of the moving average algorithm.

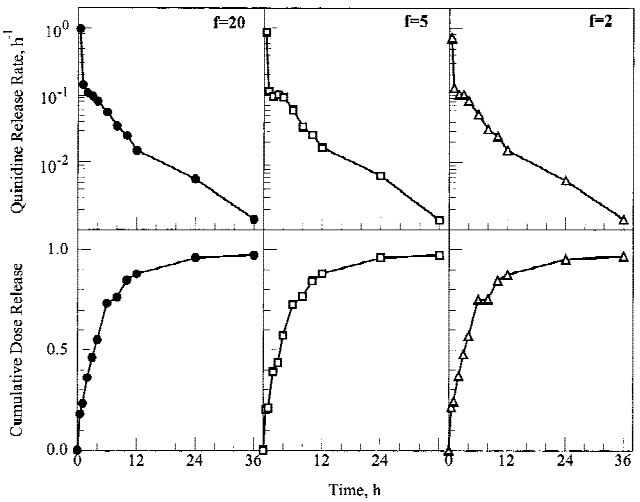

Fig. 4. Drug release rate (upper panel) and cumulative release profiles (lower panel) of quinidine sustained release formulation relative to the oral solution (21). These results suggests the apparent drug release from the formulation was polyphasic. Varying the subdivision parameter from $f = 20$ (●) to $f = 5$ (□) or 2 (△) yielded comparable profiles. Without reducing the step-size ($f = 1$; Table V), significant oscillations in the release profile were noted over the first 2 h post-dose.

With the availability of modern analytical technology and instrumentation, there has been a significant improvement in the quality of assay data in recent years. In the presence of experimental errors at levels commonly encountered in validated assay procedures (22), the application of the present method has been shown to yield satisfactory absorption rate profiles. In actual practice, where the precise magnitudes of assay noise and input rate profiles are not known, preliminary analysis of the data with larger-step sizes (e.g., $f = 1$), followed by additional analysis with smaller step-sizes has been found to serve as a practical guide in judging the acceptability of the computed rate estimates.

In conclusion, the point-area deconvolution analysis is one of the preferred approaches in evaluating pharmacokinetic and biopharmaceutic data when it is undesirable to assume the functional forms of the input processes. The present method provides improved performance and flexibility of this approach. Software implementing the computational procedures is available upon request.

APPENDIX

In a linear and time-invariant disposition system, plamsa concentration data $c(t)$ following a bolus intravenous dose are often represented by a polyexponential function of the form:

$$c(t) = \sum_{i=1}^{M} a_i e^{-\lambda_i t} \tag{A1}$$

where M is the number of the exponential terms. In such a case, the piecewise cubic polynomial functions are not applied to interpolate the impulse response data; the b_{jk} terms shown in Eq. 11 are obtained by analytical integration of Eq. A1:

$$b_{jk} = \sum_{i=1}^{M} \frac{a_i}{\lambda_i}[e^{-\lambda_i(t_j - t_{k-1})} - e^{-\lambda_i(t_j - t_k)}] \quad \text{(A2)}$$

In comparison to the use of the polynomial interpolation of i.v. data, the use of a polyexponential function in Eq. A2 provides an implicit smoothing and a reduction of the effect of experimental errors on the i.v. data.

REFERENCES

1. T. Prueksaritanont, L. M. Gorham, and K. C. Yeh. Analysis of metabolite kinetics by deconvolution and *in vivo-in vitro* correlations of metabolite formation rates: studies of fibrinogen receptor antagonist ester prodrug. *J. Pharm Sci.* **86**:1345–1351 (1997).
2. M. Hanano. Studies on absorption and excretion of drugs. VII. A new estimation method for the release of drugs from dosage forms and the availability in vivo. *Chem. Pharm. Bull.* **15**:994–1001 (1967).
3. D. J. Cutler. Numerical deconvolution by least squares: use of polynomials to represent the input function. *J. Pharmacokinet. Biopharm.* **6**:243–263 (1978).
4. R. Hovorka, M. J. Chappell, K. R. Godfrey, F. N. Madden, M. K. Rouse, and P. A. Soons. CODE: A deconvolution program implementing a regularization method of deconvolution constrained to non-negative values. Description and pilot evaluation. *Biopharm. Drug Dispos.* **19**:39–53 (1998).
5. M. K. Charter and S. F. Gull. Maximum entropy and its application to the calculation of drug absorption rates. *J. Pharmacokinet. Biopharm.* **6**:645–655 (1987).
6. D. Verrota. Estimation and model selection in constrained deconvolution. *Ann. Biomed. Eng.* **21**:605–620 (1993).
7. P. Veng-Pedersen. Model-independent method of analyzing input in linear pharmacokinetic systems having polyexponential impulse response II: numerical evaluation. *J. Pharm. Sci.* **69**:305–311 (1980).
8. D. P. Vaughan. Approximation in point-area deconvolution algorithm as mathematical basis of empirical instantaneous midpoint-input deconvolution method. *J. Pharm. Sci.* **70**:831–832 (1981).
9. P. Veng-Pederson and N. Modi. An algorithm for constrained deconvolution based on reparametrization. *J. Pharm. Sci.* **81**:175–180 (1992).
10. F. N. Madden, K. R. Godfrey, M. J. Chappell, R. Hovorka, and R. A. Bates. A comparison of six deconvolution techniques. *J. Pharmacokinet. Biopharm.* **24**:283–299 (1996).
11. Z. Yu, S. S. Hwang, and S. K. Gupta. DeMonS—a new deconvolution method for estimating drug absorbed at different time intervals and/or drug disposition model parameters using a monotonic cubic spline. *Biopharm. Drug Dispos.* **18**:475–487 (1997).
12. D. P. Vaughan and M. Dennis. Mathematical basis of point-area deconvolution method for determining *in vivo* input functions. *J. Pharm. Sci.* **67**:663–665 (1978).
13. J. H. Proost. Application of a numerical deconvolution techniuqe in the assessment of bioavailability. *J. Pharm. Sci.* **74**:1135–1136 (1985).
14. K. Iga, Y. Ogawa, T. Yashiki, and T. Shimamoto. Estimation of drug absorption rates using a deconvolution method with nonequal sampling times. *J. Pharmacokinet. Biopharm.* **14**:213–225 (1986).
15. A. Deslands, J. F. Westphal, J. H. Trouvin, and R. Farinotti. Adaptive computer program for determination of absorption profiles by numerical deconvolution: application to amoxicillin absorption. *J. Pharm. Sci.* **81**:802–807 (1992).
16. D. Verotta. Two constrained deconvolution methods using spline functions. *J. Pharmacokinet. Biopharm.* **21**:609–636 (1993).
17. K. C. Yeh and R. D. Small. Pharmacokinetic evaluation of stable piecewise cubic polynomials as numerical integration functions. *J. Pharmacokinet. Biopharm.* **17**:721–740 (1989).
18. F. N. Fritsch and J. Butland. A method of constructing local monotone piecewise cubic interpolants. *Siam. J. Sci. Stat. Comput.* **5:**300–304 (1984).
19. K. C. Yeh and K. C. Kwan. Scientific commentary: a comparison of numerical integrating algorithms by trapezoidal, Lagrange, and spline approximation. *J. Pharmcokinet. Biopharm.* **6**:79–98 (1978).
20. D. V. D'Argenio. Optimal sampling times for pharmacokinetic experiments. *J. Pharmacokinet. Biopharm.* **9**:739–756 (1981).
21. W. T. Sawyer, C. C. Pulliam, A. Mattocks, J. Foster, B. W. Hadzija, and H. M. Rosenthal. Bioavailability of a commercial sustained-release quinidine tablet compared to oral quinidine solution. *Biopharm. Drug Dispos.* **3**:301–310 (1982).
22. V. P. Shah, K. K. Midha, J. W. A. Findlay, H. M. Hill, J. D. Hulse, I. J. McGilveray, G. McKay, K. J. Miller, R. N. Patnaik, M. L. Powell, A. Tonelli, C. T. Viswanathan, and A. Yacobi. Bioanalytical method validation: a revisit with a decade of progress. *Pharm. Res.* **17**:1551–1557 (2000).